Biosensors and Bioelectronics 142 (2019) 111562

Contents lists available at ScienceDirect

Biosensors and Bioelectronics

journal homepage: www.elsevier.com/locate/bios

Construction of well-ordered electrochemiluminescence sensing interface using peptide-based specific antibody immobilizer and N-(aminobutyl)-N-(ethylisoluminol) functionalized ferritin as signal indicator for procalcitonin analysis

Lei Yang[a], Jingwei Xue[a], Yue Jia[a], Yong Zhang[a], Dan Wu[a], Hongmin Ma[a], Qin Wei[a,*], Huangxian Ju[a,b]

[a] Key Laboratory of Interfacial Reaction & Sensing Analysis in Universities of Shandong, School of Chemistry and Chemical Engineering, University of Jinan, Jinan, 250022, PR China

[b] Key Laboratory of Analytical Chemistry for Life Science, School of Chemistry and Chemical Engineering, Nanjing University, Nanjing, 210023, PR China

ARTICLE INFO

Keywords:
Electrochemiluminescence
Ferritin
Polyaniline
Heptapeptide
Procalcitonin

ABSTRACT

With the aim of providing a powerful analytical tool for early diagnostics of procalcitonin (PCT), an ultrasensitive electrochemiluminescence (ECL) biosensor was developed based on a 3D well-ordered sensing interface and biocompatible signal indicator. Polyaniline nanorod arrays grafted reduced graphene oxide (PANI NRs/rGO) was hybridized with gold nanoparticles (PANI NRs/rGO-Au) as sensing substrate. To improve the specificity, HWRGWVC heptapeptide (HWR) as specific capture-antibody (Ab_1) immobilizer was introduced to construct a PANI NRs/rGO-Au-HWR sensing interface. Due to their synergistic effect, the proposed interface improved the incubation efficiency of antibody on substrate with faster electron-transfer for remarkable ECL enhancement. Then, ferritin (Ft) with superiority of biocompatibility was utilized to crosslink with ECL luminophore of *N*-(aminobutyl)-*N*-(ethylisoluminol) (ABEI-Ft) as signal indicator. ABEI-Ft exhibited high ECL efficiency and could capture detection-antibody (Ab_2) via amine reaction. Due to the enzyme-mimic property of ferric nanocore inside of Ft, abundant reactive oxygen species (ROSs) were produced in the presence of hydrogen peroxide, which further enhanced the ECL signals. On the basis, a novel biosensor was developed using PANI NRs/rGO-Au-HWR as specific sensing interface and ABEI-Ft as signal label, which performed sensitive response to PCT concentration with a wide linear range of 100 fg/mL- 50 ng/mL and a detection limit of 54 fg/mL.

1. Introduction

Sepsis as a serious systemic inflammatory response (SIRS) that caused by a bacterial, viral, or fungal infection, has become a primary cause of death due to highly variable, nonspecific and heterogeneous clinical symptoms that occurred during sepsis progression (Lim et al., 2017). Such delay in diagnosis invariably leads to an increase in patient mortality. As a typical biomarker of sepsis in human serum, procalcitonin (PCT) plays a crucial role in realizing the accurate and reliable sepsis diagnostics in the early stage (Liu et al., 2014a, b, c). To date, only several methods have been applied to analyze PCT in human serum, including electrochemical sensor, surface plasma resonance (SPR) sensor and imaging ellipsometry (IE) sensor (Liu et al., 2014; Nie et al., 2019; Sener et al., 2013; Yang et al., 2018). It can be included that new methods with higher sensitivity for the quick and dynamic concentration response of PCT in human serum are still urgently demanded.

As a powerful analytical technique, electrochemiluminescence (ECL) has drawn widespread concerns in the fields of biomarkers analysis, food safety analysis and environmental pollutant monitoring, which owns merits of high sensitivity, low background noise, wide dynamic response range and favorable controllability (Luo et al., 2018; Ma et al., 2017; Yang et al., 2017a; Yang et al., 2017b; Zhang et al., 2018). As a derivative of luminol, *N*-(aminobutyl)-*N*-(ethylisoluminol) (ABEI) is a terrific ECL reagents that can generate strong ECL emissions in the presence of hydrogen peroxide (H_2O_2) (Jiang et al., 2017; Liu et al., 2016; Yang et al., 2017). To afford a qualified biocarrier, biomaterials like DNA scaffolds and protein nanocages have been comprehensively explored for ECL luminophores loading, which greatly improves the biocompatibility of the biosensors (Tang et al., 2011;

* Corresponding author.
E-mail address: sdjndxwq@163.com (Q. Wei).

https://doi.org/10.1016/j.bios.2019.111562
Received 18 June 2019; Received in revised form 20 July 2019; Accepted 1 August 2019
Available online 02 August 2019
0956-5663/

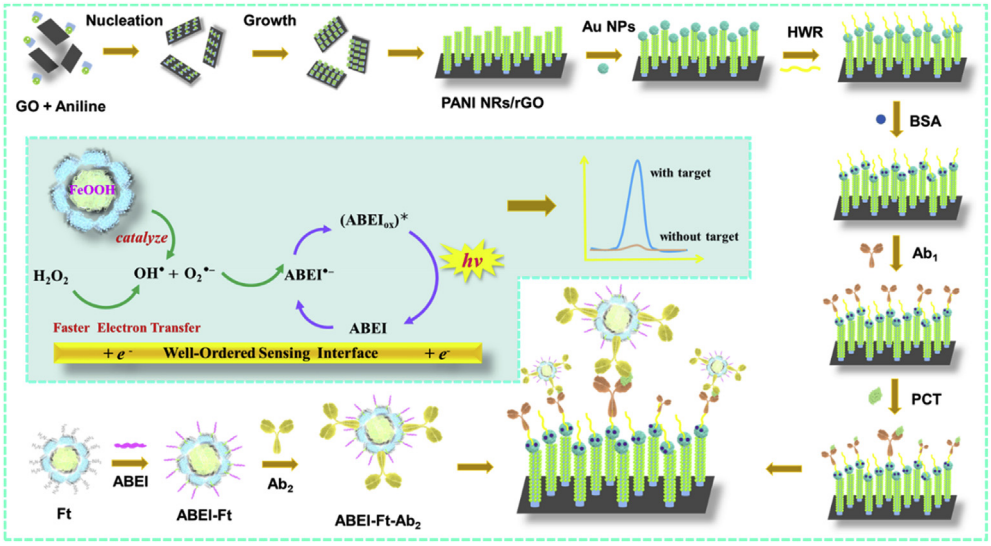

Scheme 1. Schematics diagrams of the fabrication process of the proposed ECL biosensor and possible ECL emission mechanism.

Wang et al., 2016). Ferritin (Ft), a ubiquitous iron-storage protein that encapsulates a ferric nanocore, has recently attracted growing attention in nanomaterial synthesis, nanodevices fabrication and controllable delivery of bioactive molecules due to its unique structural features, pH-tolerant property and biocompatibility (Ahn et al., 2018; Elmas et al., 2018; Fan et al., 2018; Peng et al., 2017; Zhang et al., 2017). It should be noted that, apart from its superior biocompatibility for biomolecules binding, the ferric nanocore inside of Ft possesses favorable enzyme-mimic activity that can catalyze the oxidation of luminophores in the presence of H_2O_2 (Günther et al., 2015; Tang et al., 2011). Impressed by this, Ft as a natural, catalytic and biocompatible nanocarrier was firstly served to crosslink with ABEI, which emphasized the importance of the ferric nanocore in ABEI-H_2O_2 sensing system studies.

As one of the most investigated electroactive conducting polymers, polyaniline (PANI) have been utilized in graphene-based conductive composite synthesis because of their large specific surface area, high conductivity and favorable catalytic activity (Debiemme-Chouvy et al., 2018; Jiang et al., 2018; Ke et al., 2015; Wang et al., 2017). Due to the large specific surface area and excellent electrical conductivity, reduced graphene oxide (rGO) was utilized as a conductive carrier for PANI nanorod arrays (PANI NRs) growth. By controllable synthesis, well-ordered PANI NRs were covalently grafted on rGO surface to obtain PANI NRs/rGO which exhibited superiorities than random PANI NRs growth (Liu et al., 2014). With a sufficient dense of oriented PANI NRs, all the exposed polymer parts became effective for ECL emission enhancement due to the improved electron-transport along the ordered array structure (Wu et al., 2018). Considering the above merits, PANI NRs/rGO was prepared as the perfect substrate for a 3D well-ordered ECL sensing interface construction.

As well known, antibody as a crucial specific-recognition element is necessary for immunosensing interface construction. Realizing the site-oriented immobilization of it can improve its availability for antigen binding (Makaraviciute and Ramanaviciene, 2013). To date, the developments of small peptide ligands light up the way for site-oriented antibody immobilization on nanocarriers (Dostalova et al., 2016). In particular, HWRGWV hexapeptide has been demonstrated to specifically interact with the amino acids in the loop Ser383-Asn389 (SNGQPEN) of antibody Fc fragment with high affinity (Yang et al., 2010). Our group has modified a cysteine to the C-terminal of HWRGWV hexapeptide to obtain HWRGWVC heptapeptide (HWR), which still could specifically capture antibody in a site-oriented way with high affinity (Jia et al., 2019). Possessing superiority of low cost, easy preparation, physical and chemical stability (Yang et al., 2010), HWR was employed as a powerful site-oriented antibody capturer to constructed a well-ordered specific sensing interface, which could further significantly improve the specificity and sensitivity of the biosensor.

With the aim of providing a powerful analytical tool for early diagnostics of PCT, an ultrasensitive ECL biosensor was developed based on a 3D well-ordered sensing interface and biocompatible signal indicator. First of all, ABEI was connected with Ft via glutaraldehyde (GA) crosslinking. Utilizing the superior biocompatibility of Ft, detection-antibody (Ab_2) were captured on its outer surface via amine bond. Then, the sensing interface was constructed by combining the well-ordered nanostructures of PANI NRs/rGO, the electrical and catalytic property of Au NPs and the specific interaction between HWR and antibody. PANI NRs/rGO was prepared via a facile and efficient two-step method using rGO as the conductive carrier. Abundant Au NPs were loaded on PANI NRs via Au–N bond to obtain PANI NRs/rGO-Au which could further capture HWR via Au–S bond to specifically bind with capture-antibody (Ab_1) in a site-oriented way. We proved that this interface could boost the ECL emission and accelerate the incubation process of antibody with a better maintained biological activity, which remarkably improved the sensitivity. It should be noted that PANI NRs/rGO, Au NPs, HWR peptide and ferritin are the four most crucial elements in our proposed well-ordered ECL sensing interface, the excellent synergistic effect among them contributed to the satisfying ECL performance in PCT detection. The fabrication process of the proposed biosensor was presented in Scheme 1.

2. Experimental section

2.1. Preparation of PANI NRs/rGO composite

PANI NRs/rGO composite was prepared according previous literatures with slight modifications (Liu et al., 2014). Graphene oxide (GO) was prepared by the improved Hummers' method. In typical GO-NH_2 synthesis, 100 mg GO was dispersed in 100 mL of ultrapure water by ultrasonic treatment for 1 h. Then, 30 mL of NH_3 H_2O and 30 mL of hydrazine were added into the solution to reduce GO. rGO-NH_2 was obtained by diazotization reaction for 24 h. The product was washed thoroughly with ultrapure water and dried at 80 °C. The PANI NRs/rGO composites were prepared by a low-temperature oxidation polymerization method. Briefly, 40 mg rGO-NH_2 was dispersed in 100 mL of $HClO_4$ solution (1 mol/L) by ultrasonic treatment for 1 h. Then, the mixed solution was placed at -10 °C for uniform nucleation. In order to

prevent the solution from being frozen, 25 mL of ethanol was added. Subsequently, different concentrations of aniline (0.02 mol/L, 0.04 mol/L, and 0.06 mol/L) and corresponding ammonium persulfate (3 : 2 M ratio of aniline to APS) were separately added into the above solution in ice bath. After reaction for 24 h, the product was obtained by filtering and finally dried at 60 °C.

2.2. Preparation of PANI NRs/rGO-Au-HWR composites

First of all, 2 mg/mL of PANI NRs/rGO was mixed with 1 mL of as-prepared Au NPs (preparation procedure is in **Supplementary Material**). After oscillation for 12 h, the obtained PANI NRs/rGO-Au mixture was collected by centrifugation. Then, 1 mL of HWR solution (50 ng/mL) was added into the above PANI NRs/rGO-Au mixture and oscillated for 1 h at 4 °C. After centrifugation at 10000 rpm, the sediments were dispersed into 1 mL of PBS. To block the unspecific biding sites, 400 μL of BSA solution (0.1%) was added and oscillated for 1 h at room temperature. After centrifugation and washing, the obtained PANI NRs/rGO-Au-HWR bioconjugate was added into 1 mL of pH 7.4 PBS for dispersion and then stored at 4 °C for further study.

2.3. Preparation of ABEI-Ft-Ab_2 bioconjugate

4 mL of Ft (5 μg/mL), 1.5 mL of ABEI (10 mmol/L) solution were added into a 50 mL beaker, the mixture was then diluted with 4.5 mL ultrapure water. After that, 100 μL of GA (50%) solution was added and kept stirring for 2 h to obtain the crosslinking product of ABEI-Ft. After dialyzing for another 8 h against 820 mL of NaOAc (0.1 mol/L, pH 5.5), 1 mL of PBS containing EDC (40 mM) and NHS (10 mM) was added for another 1 h of reaction. After centrifugation at 6000 rpm, the obtained solution was further incubated with 100 μL of Ab_2 solution (5 μg/mL) for 2 h under 4 °C. After centrifugation at 8000 rpm, ABEI-Ft-Ab_2 was obtained and stored at 4 °C for biosensor construction.

2.4. High performance liquid chromatography (HPLC) and circular dichroism (CD) analysis

Agilent 1260 HPLC system consisting of an UV detector and a Zorbax C18 column (4.6 × 250 mm, 5 μm) was utilized to prove the efficient combination of HWR with PANI NRs/rGO-Au via Au–S bond. Samples were eluted by using a mobile phase of acetonitrile/water (30:70, v/v). For the mobile phase, the injection volume was 10 μL with a flow rate of 0.5 mL/min, and the wavelength was set to 220 nm. Binding ratio (%) of HWR was calculated according to the following equation:

binding ratio (%) = connected HWR (ug)/ HWR (ug) × 100%

CD spectra has been demonstrated as a useful technique which is sensitive to the secondary conformation changes of protein or peptides when combined with substrate surfaces (Ianeselli et al., 2018). CD spectra was utilized to demonstrate the antibody activity after the immobilizations through HWR specific interaction and Au–N adsorption, respectively. All the CD spectra in this work were obtained by scanning from 190 to 260 nm utilizing a MOS-450 spectrometer consisting of a quartz cuvettes of 1 mm optical path length at 25 °C. All the data were expressed in terms of mean residual ellipticity (h) in deg cm^2 $dmol^{-1}$.

2.5. Fabrication of the proposed ECL biosensor

After ultrasonic cleaning with ultrapure water and ethanol, bare GCE was successively polished using 0.3 and 0.05 μm Al_2O_3 powder to a mirror-like surface. It should be noted that after each step below, the modified electrode was rinsed thoroughly with PBS (10 mmol/L, pH 7.4) to get rid of the unabsorbed species. First of all, 10 μL of PANI NRs/rGO-Au-HWR was modified onto the bare GCE surface. After that, 10 μL of Ab_1 solution (5 μg/mL) was incubated at 4 °C for 1 h. Then, 10 μL of PCT with different concentrations was incubated for 40 min at 37 °C. Finally, 10 μL of ABEI-Ft-Ab_2 was modified to form the sandwich-typed immunocomplex. Therefore, the ECL biosensor was completely constructed and stored at 4 °C for following detection.

2.6. Electrochemical and ECL measurements

Cyclic voltammetry (CV) and MPI-F ECL analyzer were employed for the electrochemical and ECL measurements, respectively. A conventional three-electrode system containing the modified GCE as working electrode, a platinum wire as counter electrode and an Ag/AgCl electrode (saturated KCl) as reference electrode was applied. The ECL detection was carried out in 10 mL of PBS (0.1 mol/L, pH 8.4) containing 45 mmol/L H_2O_2 at room temperature with parameters of photomultiplier tube voltage (800 V), scan voltage (from 0 to 0.58 V) and the scan rate (100 mV/s).

3. Results and discussion

3.1. Characterizations of PANI NRs/rGO, PANI NRs/rGO-Au and ABEI-Ft nanostructures

By regulating the concentration ratios, aniline with different concentrations (0.02-0.08 mol/L) were mixed with GO at a constant concentration of 0.4 mg/mL to prepare PANI NRs/rGO. Scanning electron microscopy (SEM) images was utilized to characterize the morphologies of PANI NRs/rGO prepared under aniline concentrations of 0.02 mol/L, 0.04 mol/L and 0.06 mol/L. Fig. 1A exhibited sparser and shorter PANI nanorods than that obtained at 0.04 mol/L (Fig. 1B). When the aniline concentration was over 0.06 mol/L, self-nucleation took place at a higher concentration which also resulted in a random nanostructure (Fig. 1C). Therefore, 0.04 mol/L was chosen as the optimal aniline concentration. Under this concentration, PANI NRs with longer length.

Were well-aligned arranging on rGO surfaces, showing a clean and well-ordered morphology in inset of Fig. 1B. Fourier transform infrared spectroscopy (FT-IR) and atomic force microscope (AFM) were applied to further prove the preparation of PANI NRs/rGO in Fig. S1. After the functionalization of Au NPs, it could be clearly seen in Fig. 1D that abundant Au NPs with an average diameter of 10 nm were distributed uniformly on the surface via Au–N bond. In addition, the morphology of pure Ft was demonstrated by negative staining TEM and high-resolution TEM (HRTEM). As shown in Fig. 1E, pure Ft with outer and inner diameter of ~12 nm and ~ 8 nm can be seen clearly. Then, the UV–vis absorption spectrum (Fig. 1F) was used to prove the synthesis of ABEI-Ft bioconjugate. The absorption peak of Ft was found at 280 nm, while the ABEI's were found at 226, 283 and 322 nm. Compared with Ft and ABEI, the absorption peaks of ABEI-Ft at 226 nm and 322 nm faded away while the absorption peak at 280 nm became wider, which indicated that ABEI molecules were connected with Ft successfully.

3.2. Advances of specific immobilization of antibody via HWR

HPLC was used to prove the efficient combination of HWR with PANI NRs/rGO-Au via Au–S bond. First of all, 1 mL of PANI NRs/rGO-Au solution were mixed with 1 mL of HWR solution (10 ng/mL) and coupled for different time at 4 °C. After centrifugation, the supernatants were collected for HLPC test and corresponding peak areas of HWR were recorded. As shown in Fig. 2A, the curves levelled off at 60 min and kept constant. According to the Peak Area = 331.2, the unconnected HRW amount was calculated to be about 2.89 ng using the regression equation $P = 32.82 + 86.19 \times \lg c$ ($R^2 = 0.995$) in Fig. S2A, which indicated that approximately 7.11 ng of HWR (71.1%) were captured via Au–S bond in 60 min. After coupling with HWR for 60 min, 10 μL of PCT Ab_1 solution (100 μg/mL) was incubated onto the PANI NRs/rGO-Au-HWR modified GCE for different time at 4 °C. When the.

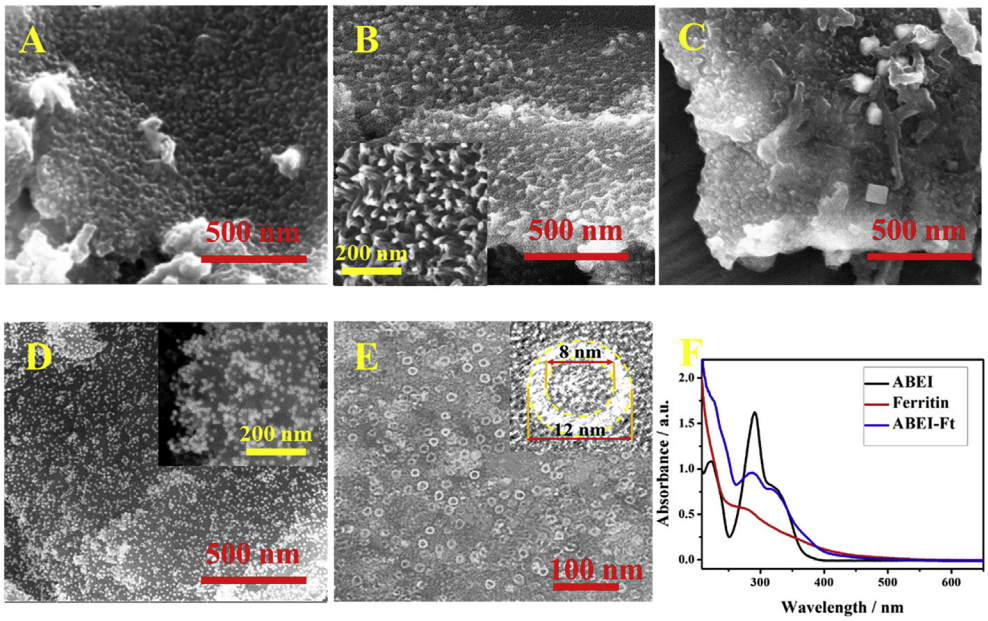

Fig. 1. SEM images of PANI NRs/rGO prepared using aniline with different concentrations: 0.02 mol/L(A), 0.04 mol/L(B), 0.06 mol/L(C). SEM image of PANI NRs/rGO-Au nanocomposite (D). Negative stain TEM image (E) and HRTEM (inset) of pure Ft stained with 2% uranyl acetate for 3 min. UV–vis absorption spectrum (F) of ABEI, Ft and ABEI-Ft.

Incubation process was done, unbounded Ab_1 were collected in 4 mL of PBS for UV–vis absorption test. As shown in Fig. 2B, the absorbance levelled off at 60 min and stayed constant. According to the absorbance (A) = 0.0212, the unconnected antibody amount was calculated to be about 0.50 μg using the regression equation $A = 0.00923 \times c + 0.00095$ ($R^2 = 0.998$) in Fig. S2B, which indicated that 0.50 μg of Ab_1 were captured by HWR in 60 min. As a comparison, 10 μL of Ab_1 solution (100 μg/mL) was incubated onto the PANI NRs/rGO-Au modified GCE for different time at 4 °C, in which Ab_1 could connect with PANI NRs/rGO-Au via Au–N adsorption. When the incubation time reached to 11 h (Fig. 2C), corresponding absorbance of 0.021 was found similar with HWR method. It should be noted that this incubation time was 9 times longer than HWR method when incubating the same amount of antibody, which revealed the advance of using HWR as an antibody capturer for shortening incubation time of antibody.

However, the biological activity maintenance of Ab_1 after using HWR and Au–N adsorption method should be investigated. Therefore, CD spectra as a reliable and rapid technique was utilized to determine the Ab_1 activity due to the fact that α-helix of secondary protein structure has specific absorption peaks at wavelength of 208 nm and 222 nm. Despite of the incubated amount of Ab_1 was same by comparing UV–vis absorbance at 280 nm, the actual activity of Ab_1 can be different using different immobilizing methods. As shown in Fig. 2D, it can be inferred that the Ab_1 activity obtained by using HWR method was better maintained than that obtained by Au–N adsorption method,

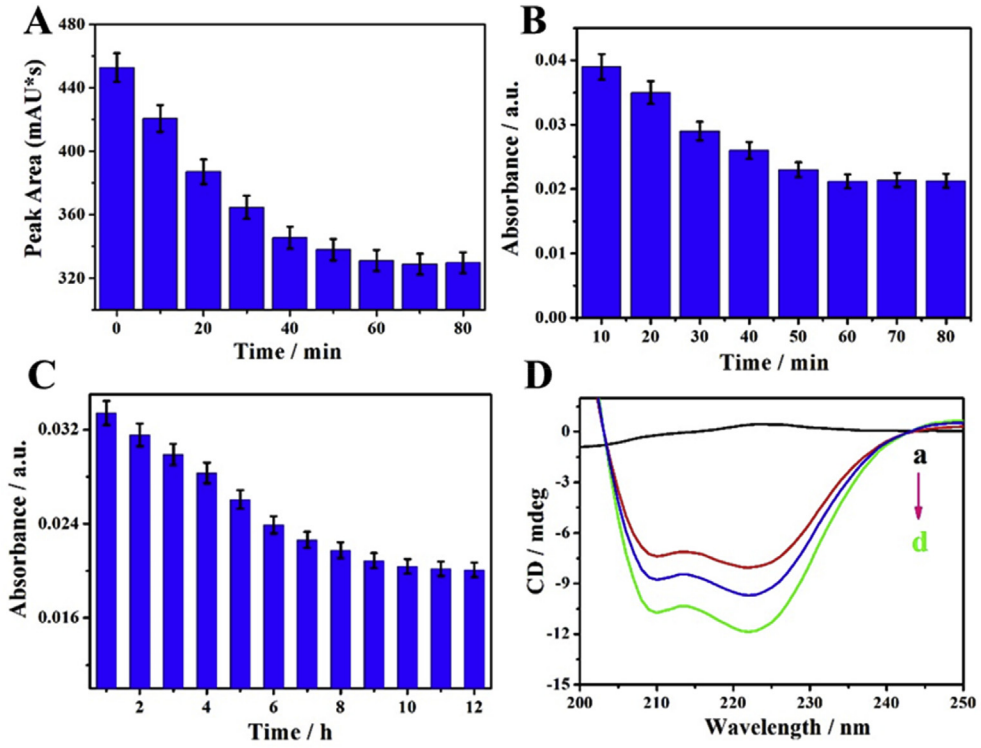

Fig. 2. (A) HPLC results of uncoupled HWR (10 ng/mL) after coupling with PANI NRs/rGO-Au from 0 to 80 min. (B) UV–vis absorption of uncaptured Ab_1 by PANI NRs/rGO-Au-HWR in a time range from 10 to 80 min. (C) UV–vis absorption spectrum of uncaptured Ab_1 by Au–N adsorption in a time range from 1 to 12 h. (D) CD spectra of pure HWR (a), PANI NRs/rGO-Au-Ab_1 (b), PANI NRs/rGO-Au-HWR-Ab_1 (c), pure Ab_1 solution(d). Error bars, SD, n = 5.

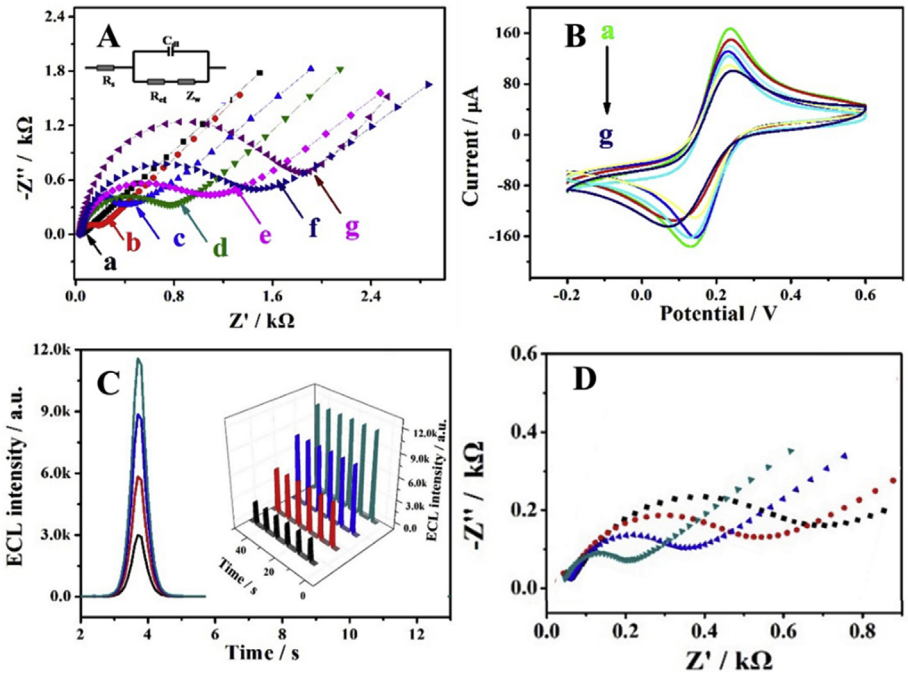

Fig. 3. (A) EIS profiles of stepwise modified electrodes in 10 mL of PBS (pH 7.4, 0.1 mol/L) containing 0.1 mol/L KCl and 5.0 mmol/L $[Fe(CN)_6]^{3-/4-}$: (a) GCE/PANI NRs/rGO-Au, (b) bare GCE, (c) GCE/PANI NRs/rGO-Au-HWR, (d) GCE/PANI NRs/rGO-Au-HWR/BSA, (e) GCE/PANI NRs/rGO-Au-HWR/BSA/Ab_1, (f) GCE/PANI NRs/rGO-Au-HWR/BSA/Ab_1/PCT, (g) GCE/PANI NRs/rGO-Au-HWR/BSA/Ab_1/PCT/ABEI-Ft-Ab_2, corresponding CV profiles of each step (B). ECL intensity-time curve (C) and EIS data (D) of biosensor based on the PANI NRs/rGO prepared under different aniline concentration: 0.02 mol/L(red line), 0.04 mol/L(blue line), 0.06 mol/L(black line) and PANI NRs/rGO-Au (green line). (For interpretation of the references to colour in this figure legend, the reader is referred to the Web version of this article.)

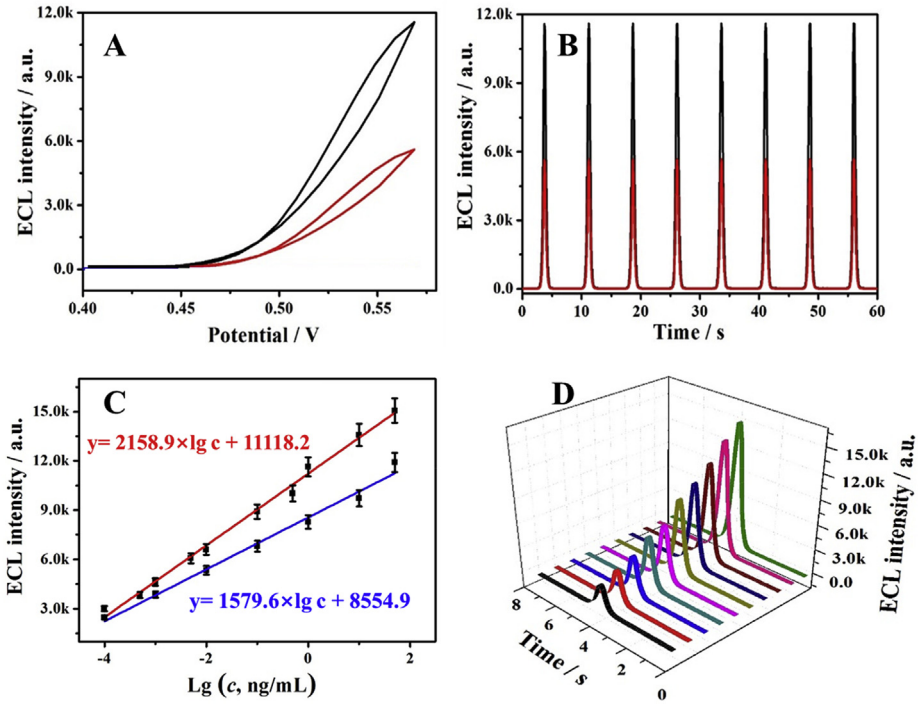

Fig. 4. ECL intensity-potential curve (A) and ECL intensity-time curve (B) of biosensors using ABEI-apoFt (5 μg/mL) and ABEI-Ft (5 μg/mL) as signal indicator, respectively. (C) Calibration curve of ECL biosensors with (red curve) and without (blue curve) HWR incubation. Corresponding ECL intensity-time curve (D) of biosensor constructed with HWR incubation. The concentration range of PCT: 100 fg/mL, 500 fg/mL, 1 pg/mL, 50 pg/mL, 100 pg/mL, 0.1 pg/mL, 0.5 ng/mL, 1 ng/mL, 10 ng/mL and 50 ng/mL. Error bars, SD, n = 5. (For interpretation of the references to colour in this figure legend, the reader is referred to the Web version of this article.)

highlighting the advance of HWR in maintaining antibody biological activity to a larger extent than conventionally used method.

3.3. Electrochemical characterizations of ECL biosensor

Stepwise characterization of the proposed biosensor was confirmed with electrochemical impedance spectroscopy (EIS) and CV profiles conducted in $[Fe(CN)_6]^{4-/3-}$ (5 mmol/L) solution containing KCl (0.1 mol/L). Impedance spectra of GCE at different modified steps was shown in Fig. 3A. PANI NRs/rGO-Au modified GCE (curve a) showed a smaller semicircle compared to bare GCE (curve b) due to the faster electron-transmission on PANI NRs/rGO-Au surface. After the continuous modifications of nonconductive HWR, BSA, Ab_1 and PCT on the GCE surface, resistance (curve c, d, e and f) increased sequentially. After the final modification of ABEI-Ft-Ab_2 bioconjugate (curve g), the resistance further increased. All the results above were consistent with the CV profiles in Fig. 3B, indicating the superficial construction of the proposed ECL biosensor was successful.

3.4. ECL emission enhancement of well-ordered sensing interface and ferric nanocore

To study the performance discrepancy of ECL biosensor caused by random and well-ordered sensing interfaces, PANI NRs/rGO was

Table 1
Recovery results of PCT in human serum samples detected by the proposed ECL biosensor.

Detected concentration (ng/mL)	Spiked concentration (ng/mL)	Theoretical concentration (ng/mL)	Found concentration (ng/mL)	Recovery/%
3.28	0.5	3.78	3.74	92.0
	3	6.28	6.24	98.6
	5	8.28	8.22	98.8
	10	13.28	13.37	100.9

prepared using aniline concentration of 0.02 mol/L, 0.04 mol/L and 0.06 mol/L. As shown in Fig. 3C, it could clearly been seen that ECL intensity reached to a higher level when the aniline concentration was 0.04 mol/L (bule line) while PANI NRs/rGO-Au (green line) exhibited the maximum ECL intensity. According to corresponding EIS data in Fig. 3D, the electrical conductivity of the well-ordered nanostructure of PANI NRs/rGO-Au was better than the others. This well-ordered interface can.

Shorten the electronic transmission path and form abundant space for full access of H_2O_2 in the electrolyte. By virtue of the facilitated electron-transfer and improved specific surface area, the decomposition of H_2O_2 was efficiently catalyzed by PANI NRs/rGO-Au to realize favorable signal-amplification.

Considering the superiority of Ft mentioned above, it is of great importance to demonstrate the natural enzyme-mimic property of the ferric nanocore. As a comparison, ABEI-apoFt (5 μg/mL) and ABEI-Ft (5 μg/mL) were employed as signal labels in the ECL biosensor construction, respectively. By comparing UV–vis absorbance at 322 nm, the cross-linked amount of ABEI on Ft and apoFt were quantified around the same level. As shown in Fig. 4A and B, ECL signal generated by ABEI@Ft (black curve, 11558 a.u.) was about 2.1 times higher than ABEI@apoFt (red curve, 5502 a.u.), which indicated the advances of using nature Ft as signal label in sensor construction. Besides, ECL signals of ABEI-Ft and ABEI-apoFt generated under different H_2O_2 concentrations were also investigated in Fig. S3. According to previous works (Liu et al., 2016; Yang et al., 2017), the possible mechanism was revealed as follows: In the anodic scanning process, ABEI molecules were chemically oxidized to obtain $ABEI^+$. Following by the quick deprotonation of $ABEI^+$, the radical anion of ABEI ($ABEI^{\bullet -}$) was generated (1). Then, PANI NRs/rGO-Au and ferric nanocore (FeOOH) facilitated the decomposition of H_2O_2 to produce more $OH^{\bullet -}$ and $O_2^{\bullet -}$ (2). As oxidants, $OH^{\bullet -}$ and $O_2^{\bullet -}$ could react with $ABEI^{\bullet -}$ to form the excited state $(ABEI_{ox})^*$(3). In the final redox process (4), $(ABEI_{ox})^*$ decayed back to the ground state to finish the ECL emission process.

$$ABEI \xrightarrow{-e^-} ABEI^+ \xrightarrow{-2H^+} ABEI^{\bullet -} \quad (1)$$

$$H_2O_2 \xrightarrow[FeOOH]{\text{PANI NRs/rGO-Au}} \text{more } OH^{\bullet} + O_2^{\bullet -} \quad (2)$$

$$ABEI^{\bullet -} + OH^{\bullet}/O_2^{\bullet -} \rightarrow (ABEI_{OX})^* + \text{products} \quad (3)$$

$$(ABEI_{OX})^* \rightarrow ABEI_{OX} + h\nu \quad (4)$$

3.5. ECL responses of biosensor toward PCT

Under the optimized experimental conditions (Fig. S4), PCT with different concentrations were detected by the proposed ECL biosensor in 10 mL of PBS (0.1 mol/L, pH 8.4) containing 45 mmol/L H_2O_2 at room temperature. ECL biosensors constructed with (red curve) and without (blue curve) HWR incubation were both measured and their relationships between ECL intensity (I_{ECL}) and logarithm of PCT concentration (lg c) were shown in Fig. 4C. Their linear relations were $I_{ECL} = 2158.9 \times \lg c + 11118.2$ ($R^2 = 0.997$) and $I_{ECL} = 1579.6 \times \lg c + 8554.9$ ($R^2 = 0.998$), respectively. It could be included that HWR was crucial in improving the sensitivity of the biosensor. This established ECL biosensor exhibited a wide linear range of 0.0001–50 ng/mL and limit of detection (LOD) of 54 fg/mL(calculation procedure is in Supplementary Material). It should be noted that the LOD of this proposed sensor was lower than other methods listed in Table S1. Moreover, this method even can be comparable to the state-of-the-art ECL sensing strategy for PCT detection, highlighting its great potential of this sensing strategy in PCT detection.

3.6. Analysis of PCT in human serum

Considering the favorable specificity, stability and reproducibility (Fig. S5), the accuracy and reliability of the biosensor were further investigated. By using standard addition method, one serum sample were divided into four groups and each group was spiked with 0.5 ng/mL, 3 ng/mL, 5 ng/mL, 10 ng/mL of PCT standard samples, respectively. As shown in Table 1, the recovery values were acceptable (92.0%–100.9%) with RSD (between 0.98% and 4.79%, n = 5), proving the potential application of the proposed biosensor in detecting PCT concentration in human serum samples.

4. Conclusion

In summary, an highly sensitive ECL biosensor was developed for PCT detection by utilizing a novel well-ordered PANI NRs/rGO-Au-HWR sensing interface and ferritin-based ECL signal indicator. PANI NRs/rGO as well-ordered interfacial substrate was firstly functionalized with Au NPs. Due to the large specific surface area, excellent electrical conductivity and catalytic property, the obtained PANI NRs/rGO-Au could efficiently catalyze the H_2O_2 decomposition to produce more ROSs, which realized remarkable ECL signal-amplification. Meanwhile, HWR as site-oriented antibody immobilizer was introduced to connect with PANI NRs/rGO-Au via Au–S bond, which facilitated the incubation process of antibody with a better maintained biological activity. Furthermore, by virtue of the excellent enzyme-mimic property of ferric nanocore, ABEI@Ft exhibited high ECL efficiency with favorable biocompatibility, which further enhanced the biosensor performance. By combining the superiorities of PANI NRs/rGO-Au-HWR with ABEI@Ft, the sensitivity of the biosensor was remarkably improved, which showed accurate response to PCT concentration in the range of 100 fg/mL-50 ng/mL with a low detection limit of 54 fg/mL. Featuring favorable specificity, stability and reproducibility, this sensing strategy lights up a new avenue for biomarkers analysis by constructing a well-ordered specific sensing interface with high sensitivity.

Declaration of competing interest

The authors declare that they have no known competing financial interests or personal relationships that could have appeared to influence the work reported in this paper.

CRediT authorship contribution statement

Lei Yang: Formal analysis, Data curation, Writing - original draft, Formal analysis, Data curation, Writing - original draft. **Jingwei Xue:** Formal analysis, Data curation, Writing - original draft. **Yue Jia:** Formal analysis, Data curation, Writing - original draft. **Yong Zhang:** Formal analysis, Data curation, Writing - original draft.

Acknowledgements

This study was supported by the National Key Scientific Instrument and Equipment Development Project of China (No. 21627809), National Natural Science Foundation of China (Nos. 21575050, 21777056, 21505051), Special Foundation for Taishan Scholar

Professorship of Shandong Province (No. ts201712052) Jinan Scientific Research Leader Workshop Project (2018GXRC024).

Appendix A. Supplementary data

Supplementary data to this article can be found online at https://doi.org/10.1016/j.bios.2019.111562.

References

Ahn, B., Lee, S.-G., Yoon, H.R., Lee, J.M., Jung, Y., 2018. Angew. Chem. Int. Ed. 57 (11), 2909–2913.
Debiemme-Chouvy, C., Fakhry, A., Pillier, F., 2018. Electrochim. Acta 268, 66–72.
Dostalova, S., Cerna, T., Hynek, D., Koudelkova, Z., Vaculovic, T., Kopel, P., Hrabeta, J., Heger, Z., Vaculovicova, M., Eckschlager, T., Stiborova, M., Adam, V., 2016. ACS Appl. Mater. Interfaces 8 (23), 14430–14441.
Elmas, S.N.K., Guzel, R., Say, M.G., Ersoz, A., Say, R., 2018. Biosens. Bioelectron. 103, 19–25.
Fan, K., Jiang, B., Guan, Z., He, J., Yang, D., Xie, N., Nie, G., Xie, C., Yan, X., 2018. Anal. Chem. 90 (9), 5671–5677.
Günther, J., Patrick, V.R., Barbara, S.M., Alexander, B.K., 2015. Chem. Rev. 115 (4), 1653–1701.
Ianeselli, A., Orioli, S., Spagnolli, G., Faccioli, P., Cupellini, L., Jurinovich, S., Mennucci, B., 2018. J. Am. Chem. Soc. 140 (10), 3674–3682.
Jia, Y., Yang, L., Feng, R., Ma, H., Fan, D., Yan, T., Feng, R., Du, B., Wei, Q., 2019. ACS Appl. Mater. Interfaces 11 (7), 7157–7163.
Jiang, X., Wang, H., Yuan, R., Chai, Y., 2018. Anal. Chem. 90 (14), 8462–8469.
Jiang, X., Wang, Z., Wang, H., Zhuo, Y., Yuan, R., Chai, Y., 2017. Chem. Commun. 53 (70), 9705–9708.
Ke, R., Zhang, X., Wang, L., Zhang, C., Zhang, S., Mao, C., Niu, H., Song, J., Jin, B., Tian, Y., 2015. J. Alloy. Compd 622, 1027–1032.
Lim, J.M., Ryu, M.Y., Kim, J.H., Cho, C.H., Park, T.J., Park, J.P., 2017. RSC Adv. 7 (58), 36562–36565.
Liu, F., Xiang, G., Chen, X., Luo, F., Jiang, D., Huang, S., Li, Y., Pu, X., 2014a. RSC Adv. 4 (27), 13934.
Liu, F., Xiang, G., Yuan, R., Chen, X., Luo, F., Jiang, D., Huang, S., Li, Y., Pu, X., 2014b. Biosens. Bioelectron. 60, 210–217.
Liu, X., Shang, P., Zhang, Y., Wang, X., Fan, Z., Wang, B., Zheng, Y., 2014c. J. Mater. Chem. A. 2 (37), 15273–15278.
Liu, Y., Wang, H., Xiong, C., Yuan, Y., Chai, Y., Yuan, R., 2016. Biosens. Bioelectron. 81, 334–340.
Luo, J.H., Cheng, D., Li, P.X., Yao, Y., Chen, S.H., Yuan, R., Xu, W.J., 2018. Chem. Commun. 54 (22), 2777–2780.
Ma, H., Zhao, Y., Liu, Y., Zhang, Y., Wu, D., Li, H., Wei, Q., 2017. Anal. Chem. 89 (24), 13049–13053.
Makaraviciute, A., Ramanaviciene, A., 2013. Biosens. Bioelectron. 50, 460–471.
Nie, R., Xu, X., Cui, X., Chen, Y., Yang, L., 2019. ACS Omega 4 (4), 6210–6217.
Peng, S., Kim, J.H., Park, S.J., 2017. J. Cryst. Growth 468, 79–83.
Sener, G., Ozgur, E., Rad, A.Y., Uzun, L., Say, R., Denizli, A., 2013. Analyst 138 (21), 6422–6428.
Tang, Z., Wu, H., Zhang, Y., Li, Z., Lin, Y., 2011. Anal. Chem. 83 (22), 8611–8616.
Wang, H., Yuan, Y., Zhuo, Y., Chai, Y., Yuan, R., 2016. Anal. Chem. 88 (11), 5797–5803.
Wang, P., Du, X., An, X., Li, S., Gao, F., Hao, X., Guan, G., 2017. Synth. Met. 232, 87–95.
Wu, D., Wei, Y., Ren, X., Ji, X., Liu, Y., Guo, X., Liu, Z., Asiri, A.M., Wei, Q., Sun, X., 2018. Adv. Mater. 30 (9), 1705366.
Yang, H., Gurgel, P.V., Williams Jr., D.K., Bobay, B.G., Cavanagh, J., Muddiman, D.C., Carbonell, R.G., 2010. J. Mol. Recognit. 23 (3), 271–282.
Yang, H.Y., Wang, H.J., Xiong, C.Y., Chai, Y.Q., Yuan, R., 2017. ACS Appl. Mater. Interfaces 9 (41), 36239–36246.
Yang, L., Li, Y., Zhang, Y., Fan, D., Pang, X., Wei, Q., Du, B., 2017a. ACS Appl. Mater. Interfaces 9 (40), 35260–35267.
Yang, L., Zhu, W., Ren, X., Khan, M.S., Zhang, Y., Du, B., Wei, Q., 2017b. Biosens. Bioelectron. 91, 842–848.
Yang, Z., Shao, X., Han, Y., Zhang, H., 2018. Anal. Methods. 10 (9), 1015–1022.
Zhang, S., Zang, J., Chen, H., Li, M., Xu, C., Zhao, G., 2017. Small 13 (37), 1701045.
Zhang, Y., Li, X., Xu, Z., Chai, Y., Wang, H., Yuan, R., 2018. Chem. Commun. 54 (72), 10148–10151.